A NEW SOLUTION ALGORITHM FOR HEAT TRANSFER IN VERTICAL ANNULAR TWO-PHASE FLOW

A. Alvarez Toledo, alvareztoledoa@yahoo.com
E. E. Paladino, emilio@ct.ufrn.br
F. M. Fernández, fernandez.lubnicki@gmail.com

Graduate Program in Mechanical Engineering, Universidade Federal de Rio Grande do Norte, Natal, RN 59072-970, Brazil

Abstract. *This work presents a numerical model for solving the thermal entry problem in vertical, annular, two-phase flow. The momentum and energy equations are solved to obtain the velocity and temperature fields in both the core and the film. Each equation is solved for the core and the film simultaneously using the Finite Volume Method and an iterative procedure is employed to deal with the well known coupling in annular flows, between the film velocity, shear stress and film thickness. For the thermal entry problem, three types of boundary conditions can be used, namely prescribed temperature, prescribed wall heat flux, or mixed type. The Nusselt number and the heat transfer coefficient are computed from the temperature profile along the axial position for these cases.*

Keywords: *Annular flow, Finite Volume Method, Heat transfer*

1. INTRODUCTION

Annular two-phase flow is one of the most common configurations in multiphase flows. It occurs in both, gas-liquid and liquid-liquid systems for laminar and turbulent regimes. Regarding gas-liquid annular flow, it is commonly encountered in the process, nuclear and oil industries, inside boilers and heat exchangers, for example. It occurs at moderate to high gas superficial velocities and it is characterized by the existence of a liquid film adjacent to the wall and a gas core flowing in the center of the duct. A wavy interface exists between both phases and its morphology depends on the gas and liquid mass flow rates (see for example Azzopardi, 1997; Whalley & Hewitt, 1978). This flow pattern has been widely studied because it is preferred in many processes due to its large convective heat transfer coefficient. Furthermore, it usually occurs before critical heat flux is reached in evaporative heat-transfer systems (Hewitt & Whalley, 1989). As far as liquid-liquid annular flow is concerned, it has attracted interest in the oil industry because of the proved enhanced efficiency of the water lubricated transportation of heavy oils; water is injected in the oil such that it flows as an annular film along the pipe wall while oil flows in the core (see Ghosh *et al.*, 2009). In liquid-liquid annular flow, the interface is not always wavy as in gas-liquid, but other aspects regarding stability are important (see Bannwart, 2001). Other benefits, like corrosion prevention in aqueous liquid solutions transportation, for example, can be obtained by liquid-liquid annular flow.

The hydrodynamic problem in annular two-phase flow has been widely studied and various models have been proposed. Yet, their scope is usually limited to either liquid-liquid or gas-liquid systems, as they rely on empirical closure relations or are based on restrictive hypothesis upon flow regime, film thickness or shear stress distributions Beyond stability issues and interfacial phenomena, annular flow in both types of systems can be modeled using the same approach, since they can be described by a unique set of governing equations, momentum, mass and energy conservation equations. As pointed out by Hewitt & Whalley (1989), given the independent variables (fluid properties, channel geometry and total core and film flow rates), annular flow modeling consists in the calculation of three dependent variables, namely film flow rate, mean film thickness, and pressure gradient(or wall shear stress).

Laminar annular flow is rarely encountered in gas-liquid systems, so models for this pattern have to take into account the gas core and liquid film turbulence, and the complex interaction across the interface. In addition, other phenomena as entrainment and deposition are to be contemplated (see (Moeck & Stachiewicz 1972); (Dobran 1983); Adechy & Issa, 2004; Kishore & Jayanti, 2004; Antal *et al.,* 1998; Okawa *et al.,* 2000; Alipchenkov *et al.,* 2004, among others). Whereas in liquid-liquid systems, there is a wide range of flow rates for which the flow can be laminar. In these cases, if the film thickness and the pressure gradient are known, the analytical solution can be obtained.

The heat transfer problem has been studied for laminar liquid-liquid flow using the analytical solution of the momentum equations to obtain the velocity fields necessary to solve the energy equation (Stockman & Epstein, 2001; Su, 2006; Leib *et al.,* 1971). These works solve the energy equation analytically for different boundary conditions at the wall. Some works (Dobran, 1983; Fu & Klausner, 1997) solve the energy equation for gas-liquid annular flow using a separate hydrodynamic model for each phase and closure relations for the interface which depend on empirical correlations for the interfacial or wall shear stress.

Fernández *et al.* (2010) developed a model to solve the hydro-dynamically fully developed flow in annular two-phase flow. This work presents a new solution algorithm which, unlike mentioned approaches, makes no use of empirical closure correlations to relate shear stresses, pressure gradient and film thickness nor assumes any velocity profile for the film. It provides an accurate, simple and complete numerical computation of all the hydrodynamic

parameters requiring just core and film fluid mass flow rates as input data to solve mass and momentum conservation equations. The success of the algorithm relies on two main features, (1) the coupled solution of the film and core velocity fields, which inherently satisfies the continuity of the velocity and shear stress fields at the interface, and (2) the pressure gradient calculation through an iterative procedure based on the fulfillment of the global mass conservation of the core.

The main objective of this work is to complement the solution presented in Fernández et al (2010) by developing a complete model for the numerical solution of the energy equation in annular flow, which can be solved either for gas-liquid or liquid-liquid systems, as well as for laminar or turbulent flow regimes, as long as a suitable model for effective viscosity and conductivity calculation is incorporated. The energy equation can be solved for any of the three kinds of boundary conditions. The solution of the energy equations for the core and film described below, is based on the same approach used for the momentum equations. This method solves the momentum and energy equations for the core and film in a coupled way automatically satisfying the shear stress and heat flux at the interface.

The model is validated against the solutions given by Leib *et al.* (1971) and Su (2006) for liquid-liquid laminar annular flow.

2. HYDRODYNAMICS

The flow field for hydro-dynamically fully developed, laminar, two phase flow with smooth interface is illustrated in figure 1. The subscripts c and f stand for core and film respectively. The velocity fields $U_f(R)$ and $U_c(R)$ in figure 1 are merely illustrative. R is the tube radius and δ is the mean film thickness.

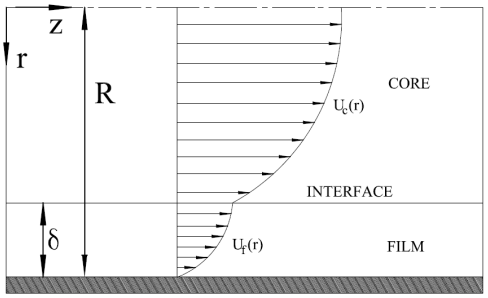

Figure 1: Core-annular flow of two fluids in a circular pipe

The equations that describe the velocity fields, written for cylindrical coordinates, are

$$\frac{1}{r}\frac{d}{dr}\left(\mu_c\, r\,\frac{du_c}{dr}\right)=\frac{dp}{dz}-\rho_c g \qquad 0<r<R-\delta \tag{1}$$

$$\frac{1}{r}\frac{d}{dr}\left(\mu_f\, r\,\frac{du_f}{dr}\right)=\frac{dp}{dz}-\rho_f g \qquad 0<r<R-\delta \tag{2}$$

where μ_c , ρ_c, μ_f and ρ_f are the dynamic viscosities and densities of the core and the film. The momentum equations are subject to the following boundary conditions,

$$\frac{du}{dr}=0 \qquad r=0 \tag{3}$$

$$u=0 \qquad r=R \tag{4}$$

The continuity of velocities and shear stresses at interface is respectively given by Eqs. (5) and (6).

$$u_c(R-\delta)=u_f(R-\delta)=u_I \tag{5}$$

$$\tau_c\big|_{R-\delta}=\tau_f\big|_{R-\delta}=\tau_I \tag{6}$$

The mass flows of core and film are calculated by the integration of the velocity profiles as,

$$\dot{m}_c = 2\pi\rho_c \int_0^{R-\delta} u(r)\cdot r dr \tag{7}$$

$$\dot{m}_f = 2\pi\rho_f \int_{R-\delta}^{R} u(r)\cdot r dr \tag{8}$$

These relations represent the global mass conservation for the core and film and are used, together with momentum conservation, in an iterative solution algorithm to correct and obtain the pressure gradient and the film thickness that satisfy the mentioned equations, for given superficial velocities.

3. HEAT TRANSFER

The steady state heat transfer in the thermal entry region for annular flow, disregarding axial diffusion and viscous dissipation, is governed by the following equations.

$$\frac{\partial\left(\rho_c \cdot cp_c \cdot u \cdot T_c\right)}{\partial z} = \frac{1}{r}\frac{\partial}{\partial r}\left(k_c \cdot r \cdot \frac{\partial T_c}{\partial r}\right) \qquad 0 < r < R-\delta \tag{9}$$

$$\frac{\partial\left(\rho_f \cdot cp_f \cdot u \cdot T_f\right)}{\partial z} = \frac{1}{r}\frac{\partial}{\partial r}\left(k_f \cdot r \cdot \frac{\partial T_f}{\partial r}\right) \qquad R-\delta < r < R \tag{10}$$

where k_c, cp_c, k_f and cp_f are the core and film conductivities and specific heat. The initial condition for temperature is given by,

$$T(0,r) = T0 \tag{11}$$

The boundary condition at the center of the tube is,

$$\frac{dT}{dr} = 0 \qquad r = 0 \tag{12}$$

The continuity of fluxes at interface gives,

$$q_c''\big|_{R-\delta} = q_f''\big|_{R-\delta} \tag{13}$$

The boundary conditions at the wall can be:

1. First kind boundary condition, prescribed temperature,

$$T(z,R) = Tw \tag{14}$$

2. Second kind boundary condition, prescribed wall flux,

$$-k_f \left.\frac{\partial T}{\partial r}\right|_{r=R} = q_w'' \tag{15}$$

3. Third kind boundary condition, heat transfer with an external fluid of temperature *Ta* and heat transfer coefficient *h*,

$$-k_f \frac{\partial T(z,R)}{\partial r} = h\cdot[T(z,R) - Ta] \tag{16}$$

4. FINITE VOLUME INTEGRATION

The time-averaged transport equations for both the core and the film are integrated along their entire domains. An independent mesh with a fixed number of volumes for each region allows refinement within the film. The interface

between both phases is positioned between the last core volume (*Ng*) and the first film volume (*Ng+1*), as shown in Figure 2. Along the iterative procedure of the algorithm explained in Section 5, the film thickness varies each time it is corrected, so *Δrl* and *Δrg* are adjusted as well since the number of volumes within the film and the core is constant.

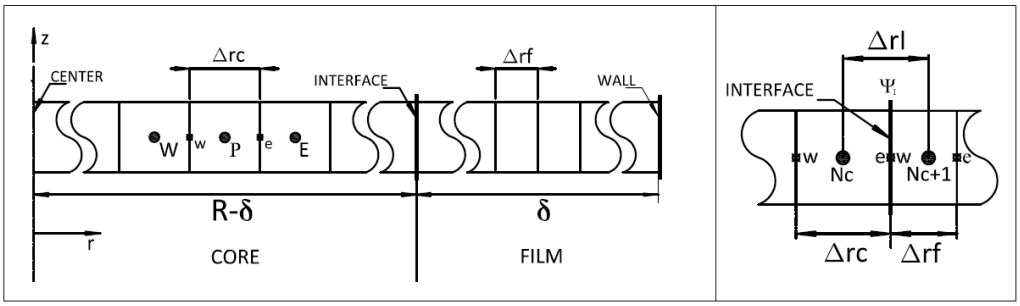

Figure 2: (a) Grids for core and film domains – (b) Finite volumes contiguous to the interface

The transport equations (1), (2), (9) and (10) are written for a generic transported variable Φ with its corresponding diffusion coefficient Γ.

$$\frac{\partial\left(I^{\phi}\cdot u\cdot\phi\right)}{\partial z}=\frac{1}{r}\frac{\partial}{\partial r}\left(\Gamma\cdot r\cdot\frac{\partial\phi}{\partial r}\right)\quad+\quad S \tag{17}$$

As the problem is hydro-dynamically fully developed, the advective term in equation 17 is zero. The generic variables are summarized in Table 1 for each one of the transport equations. The greek letter Ψ stands for shear stresses and heat flux that will later be referred to in a generic way. The generic property I^{Φ} is the thermal and momentum inertia.

Table 1: Transported variables and transport properties

	ϕ	Γ	I^{ϕ}	S	Ψ
Momentum	Uz	μ	ρ	$-\frac{dp}{dz}+\rho g$	τ
Energy	T	k	$\rho\cdot cp$	0	$q"$

Integration of Eq. (17) in volume P (Figure 2) gives,

$$r_p\Delta r\left[(\rho\,U\,\phi)\big|_n-(\rho\,U\,\phi)\big|_s\right]=r_e\underbrace{\Gamma\frac{d\phi}{dr}\bigg|_e}_{\Psi_e}-r_w\underbrace{\Gamma\frac{d\phi}{dr}\bigg|_w}_{\Psi_w}+S\frac{(r_e^{\,2}-r_w^{\,2})}{2} \tag{18}$$

Equation (18) is valid for internal volumes in both fields, the film and the core, as long as the physical properties and the volume size of each field are used. For interpolating the derivatives in the diffusive terms, central differencing scheme (CDS) is used. In turn, upwind scheme is used for advective terms, since energy diffusion in axial direction is neglected. The southern term adds to the source term as shown in Table 2. This means that the thermal entry problem is solved in a parabolic way, solving one slice at a time before moving on to the next one. After interpolation is done, the following algebraic equation represents the discrete momentum conservation within volume P.

$$A_p\phi_P+A_e\phi_E+A_w\phi_W=\quad B \tag{19}$$

The coefficients for equation (19) are shown in Table 2.

Table 2: Coefficients for internal volumes

	A_p	A_e	A_w	B
Momentum	$\frac{\mu_e r_e}{\Delta r}+\frac{\mu_w r_w}{\Delta r}$	$-\frac{\mu_e r_e}{\Delta r}$	$-\frac{\mu_w r_w}{\Delta r}$	$-\frac{dp}{dz}\frac{r_e^{\,2}-r_w^{\,2}}{2}$
Energy	$\frac{k_e r_e}{\Delta r}+\frac{k_w r_w}{\Delta r}+\frac{\rho\cdot cp\cdot U_P}{\Delta z}\cdot\left(\frac{r_e^{\,2}+r_w^{\,2}}{2}\right)$	$-\frac{k_e r_e}{\Delta r}$	$-\frac{k_w r_w}{\Delta r}$	$\frac{\rho\cdot cp\cdot U_P}{\Delta z}\cdot\left(\frac{r_e^{\,2}+r_w^{\,2}}{2}\right)\cdot T_S$

To integrate Eq.(17) within volumes contiguous to the interface, *Nc* and *Nc+1* in Figure 2, the continuity of interfacial stresses and heat fluxes has to be ensured by finding a single expression to evaluate them in both volumes as equation (20) illustrates.

$$\underbrace{\Gamma_c \left.\frac{du_c}{dr}\right|_{R-\delta}}_{\Psi_{e(Nc)}} = \underbrace{\Gamma_f \left.\frac{du_f}{dr}\right|_{R-\delta}}_{\Psi_{w(Nc+1)}} = \Psi_I \tag{20}$$

To accomplish this, a procedure described in Patankar (1980) for media with non-uniform diffusion coefficient (say viscosity or conductivity) is used. An expression for an equivalent interfacial diffusivity is derived out of the continuity of Ψ at the interface resulting in,

$$\Gamma_e = \left(\frac{1-f_e}{\Gamma_P}+\frac{f_e}{\Gamma_E}\right) \quad ; \quad f_e = \frac{\Delta r_f}{\Delta r_f + \Delta r_c} \tag{21}$$

Then, Ψ is calculated as,

$$\Psi_I = \Gamma_I \left.\frac{d\phi}{dr}\right|_I = \Gamma_I \frac{\phi_E - \phi_P}{\Delta r_I} \tag{22}$$

where $\Delta r_I = \frac{1}{2}\left(\Delta r_c + \Delta r_f\right)$

The interpolation of the derivative at the interface is done by CDS using the velocities of interfacial volumes, *Nc* and *Nc+1*, as shown by Eq.(21). While the advective and source terms remain the same, the diffusive terms of the coefficients A^D for the discretized momentum equations for volumes *Nc* and *Nc+1* are,

Table 3: Diffusion terms of the coefficients for interfacial volumes

	A_P^D	A_e^D	A_w^D
Volume Nc	$\frac{\Gamma_I r_e}{\Delta rI}+\frac{\Gamma_{Nc} r_w}{\Delta rc}$	$-\frac{\Gamma_I r_e}{\Delta rI}$	$-\frac{\Gamma_{Nc} r_w}{\Delta rc}$
Volume Nc+1	$\frac{\Gamma_I r_w}{\Delta rI}+\frac{\Gamma_{Nc+2} r_e}{\Delta rf}$	$-\frac{\Gamma_{Nc+2} r_e}{\Delta rc}$	$-\frac{\Gamma_I r_w}{\Delta rI}$

The diffusivity is stored at the volume faces in a staggered grid to simplify discretization since it is required at the volume interfaces to calculate fluxes. It is expressed as a split function (24).

$$\Gamma = \begin{cases} \Gamma_c & 0 < r < R-\delta \\ \Gamma_f & R-\delta < r < R \\ \\ \dfrac{1-f_I}{\Gamma_c}+\dfrac{f_I}{\Gamma_f} & R=\delta \end{cases} \tag{23}$$

Velocity and temperature fields for the film the core are solved in a single matrix equation simultaneously, as schematically shown below, satisfying the momentum and energy equations and boundary conditions, for given pressure gradient and film thickness.

$$\begin{bmatrix} A_c^{\phi} & \ddots \\ \ddots & A_f^{\phi} \end{bmatrix} \begin{bmatrix} \phi_c \\ \phi_f \end{bmatrix} = \begin{bmatrix} B_c \\ B_f \end{bmatrix} \tag{24}$$

5. SOLUTION ALGORITHM

The flow chart shown in Figure 4 summarizes the scheme of solution. The input data consist in mass flow rates of each phase, fluid properties, tube dimensions, initial conditions and numerical parameters such as convergence tolerance and mesh size. Initial values of pressure gradient and film thickness need to be guessed. These are corrected through an iterative procedure until the converged values are obtained.

The hydrodynamic solution is first solved in order to obtain the velocity fields necessary for the thermal entry problem. For a given film thickness, the external loop starts calculating the position of the volume centers and faces for the whole domain, core and film. It also builds a deferred mesh for viscosity. Then, for a given pressure gradient, the internal loop solves Eqs. (1) and (2) to obtain the velocity profiles of the film and the core. With the core field, its mass flow rate is obtained using Eq. (7) and the pressure gradient is adjusted to satisfy the known core flow rate through a procedure similar to the one proposed by (Patankar & Spalding 1972). This algorithm uses the error between the flow rate calculated from the velocities obtained from momentum equations and the given value to correct the pressure gradient. With it, new velocities are obtained from the momentum equation and the process is repeated until the core mass flow rate is satisfied. After convergence of the internal loop, the velocity fields and pressure gradient satisfy momentum equation for a given film thickness.

Next, the film thickness is corrected to satisfy the mass flow rate of the film using Eq. (8). As the number of volumes in each domain is constant, values of Δrc and Δrf change, as well as the positions of volume centers and faces. As the correction of δ affects the velocity field of both, core and film, the algorithm re-enters the internal loop, to find the pressure gradient that satisfies momentum equation for the new film thickness. This process is repeated until convergence of the whole system, obtaining velocity fields, film thickness and pressure gradient that satisfy momentum and mass conservation equations (Eqs. (1),(2),(7) and (8)).

Although this algorithm has two correction loops, it shows very quick convergence for the cases used in validation, even starting from guessed values of pressure gradient and film thickness very far from the converged ones.

It is important to highlight that the coupled solution of film and core velocity fields (Eq.25) satisfies the continuity of shear stress at the interface and provides a pressure gradient dependent upon the core mass flow rate. In turn, the pressure gradient is responsible for the film velocity field, which determines the wall shear stress. In this way, the intimate relationship between the wall shear stress and pressure gradient is fulfilled without explicitly making use of any equation to relate them within the solution process. This is one of the key points of the algorithm because the triangular relationship between the film mass flow rate, the wall shear stress, and the film thickness is successfully solved making no use of empirical relations for wall or interfacial friction factor nor assuming any film velocity profile. In addition, this feature makes the model extendible to the parabolic flow case, *i.e*, when force summation (pressure and wall shear stress) is unbalanced due to acceleration.

Once the velocity fields and the film thickness are obtained, the algorithm solves the thermal entry problem in a parabolic way. This means that one tube slice at a time is solved before moving on to the next one, where the previous temperature field is used. An axial mesh is built with a finite number of volumes *Nz* and system (25) is solved for each slice of the tube, until the temperature profile develops. The bulk temperature of each phase and that of the whole system is computed in order to get complete information for different definitions of Nusselt numbers, which is then computed, together with the heat transfer coefficient.

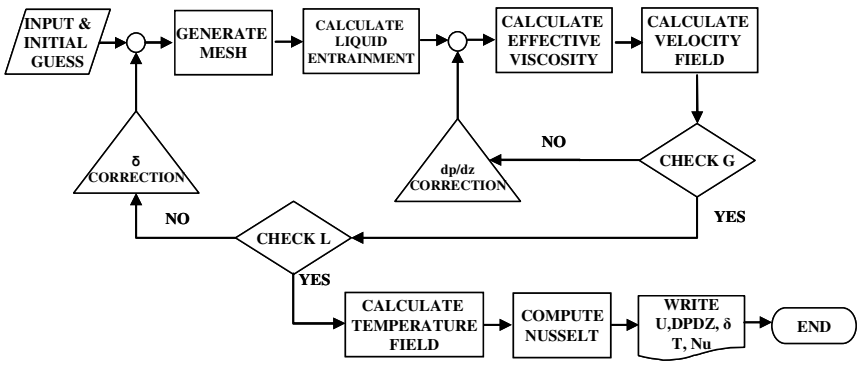

Figure 3: Flow chart for the solution algorithm

6. VALIDATION AND RESULTS

The validation of the algorithm is done in three stages. First, the hydrodynamic results are compared to the analytical solution in order to show the accuracy of the iterative procedure. Then, the temperature profiles are compared to the analytical solution obtained by Leib *et al.* (1971). Finally, the Nusselt number is computed and compared with the values obtained by Su (2006) form an analytical solution for the thermal entry problem of a viscous oil flowing in the core, and a less viscous fluid flowing in the film.

For the first two stages, the liquid-liquid system composed by water and kerosene was chosen in order to compare the current results with those of Leib *et al.* (1971) who developed a large series of experiments for different flow rate of water and kerosene and different temperatures at the entrance. Table 4 summarizes the information of the cases chosen for validation, from that work.

Table 4: Flow rates and initial temperatures

	Qc [lt/min]	Qf [lt/min]	Tc [°C]	Tf [°C]
A2	2,03	2,45	28,4	28,4
B2	2,03	2,05	28,4	28,4
C2	2,03	1,5	28,4	28,4
B5	2,7	2,05	28,5	51,9

6.1 Analytical solution

Velocity profiles obtained from the implemented algorithm using laminar viscosities are compared with the analytical solution for fully developed laminar annular flow for known pressure gradient and film thickness. This comparison shows how accurate the algorithm is, in terms of solving the triangular relationship of the film. The predicted pressure gradient and film thickness were substituted into Eqs. (25) and (26) to compare analytical profiles with the predicted ones.

$$u_c(r) = \frac{-(dP/dz + \rho_c g)}{4\mu_c}\left[(R-\delta)^2 - r^2\right] + \frac{-(dP/dz + \rho_f g)}{4\mu_f}\left[R^2 - (R-\delta)^2\right] + \frac{(R-\delta)^2}{\mu_f}(\rho_c - \rho_f) g \ln\left(\frac{R-\delta}{R}\right)^2 \quad (25)$$

$$u_f(r) = \frac{-(dP/dz + \rho_f g)}{4\mu_l}\left[R^2 - r^2\right] + \frac{(R-\delta)^2}{\mu_l}(\rho_c - \rho_f) g \ln\left(\frac{r}{R}\right)^2 \quad (26)$$

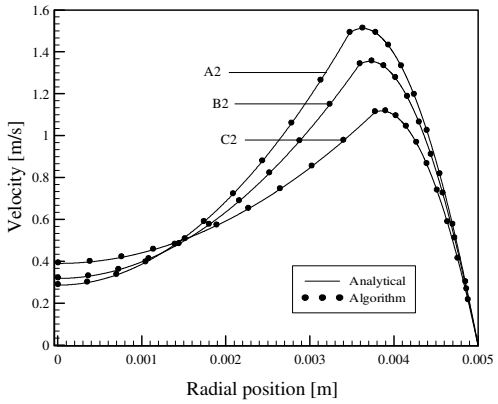

Figure 4: Algorithm results against the analytical solution

6.2 Temperature profiles

Cases A2 and B3 of table 4 were chosen to compare the results for the temperature profiles. Figures 7 a) and b) present a comparison of the temperature profiles obtained by Leib *et al.* (1971) using an analytical solution and the ones obtained by the present algorithm. The figures also show the least squares fitting curves of the experimental data presented by the reference. Nevertheless, as also reported by the reference, the experimental conditions used resulted in Reynolds number above the transition region or in fully turbulent regime. Then both, the analytical solution and the numerical hereby developed would fail in these case. The implementation of a turbulence model into the numerical algorithm is under run.

It is important to highlight that the present algorithm takes the input data presented in table 4 and solves the transport equations obtaining the velocity fields as well as the pressure gradient and the film thickness. In contrast, to obtain the velocity profiles from the analytical solution, pressure gradient and film thickness need to be known. Then, the results obtained by the algorithm are introduced in Eqs. (25) and (26) in order to compare the results given by the model against a well established solution.

The fluid properties of water and kerosene are calculated with the axial bulk temperature of each phase. As kerosene is not a pure substance, its properties can present large variations for the experimental conditions analyzed. This can explain the temperature differences between the calculated temperature profiles and those obtained by Leib *et al.* (1971) through an analytical solution, where different properties could be considered. The values of the properties used in the solution are not mentioned in Leib *et al.* (1971) work.

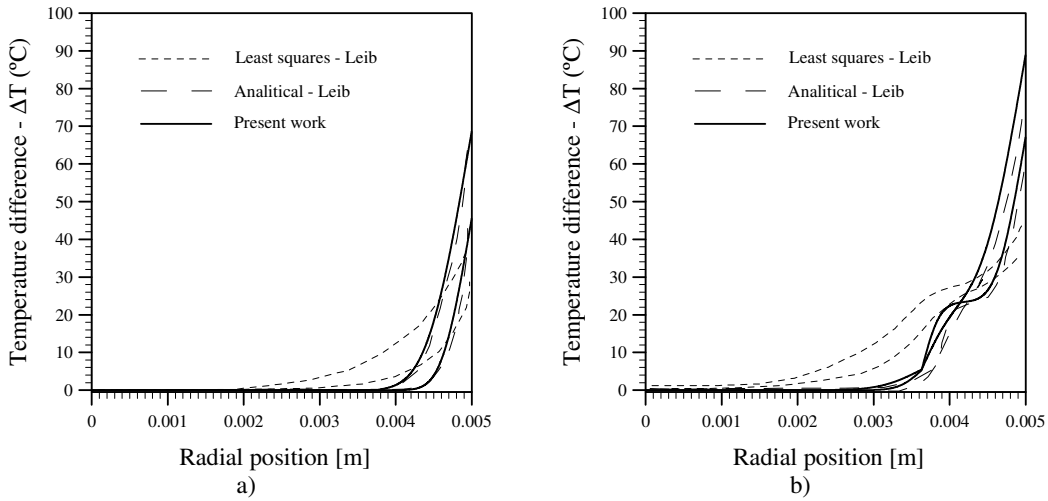

Figure 5: Radial temperature profiles comparison for the cases a) A2 and b) B5 of Leib *et al.* (1971)

6.3 Nusselt number

The system chosen to show Nusselt number results is the one that is represented by the following fluid properties relations.

$$\frac{k_f}{k_c}=5 \qquad \frac{\mu_f}{\mu_c}=0,02 \qquad \frac{\alpha_f}{\alpha_c}=0,02$$

The Nusselt number is defined as,

$$Nu(x)=\frac{-k_f\,2R\left[\partial T(x,R)/\partial r\right]}{k_c\left[Tb(x)-Tw(x)\right]} \tag{27}$$

where, the bulk temperature is defined by,

$$Tb(x)=\frac{\int_0^{R-\delta}\rho_c cp_c u(r)T(x,r)2\pi r dr+\int_{R-\delta}^{R}\rho_f cp_f u(r)T(x,r)2\pi r dr}{\int_0^{R-\delta}\rho_c cp_c u(r)2\pi r dr+\int_{R-\delta}^{R}\rho_f cp_f u(r)2\pi r dr} \tag{28}$$

The results are expressed in terms of a dimensionless variable ξ defined below.

$$\xi=\frac{x}{RPe} \qquad Pe=\frac{u_{av}2R}{\alpha_c} \qquad u_{av}=\frac{Q_c+Q_f}{\pi R^2} \qquad \alpha_c=\frac{k_c}{\rho_c cp_c} \tag{29}$$

Figure 5 show the results for Nusselt number for first and third kind boundary condition compared to the ones presented by Su (2006) using an analytical solution for the temperature profiles.

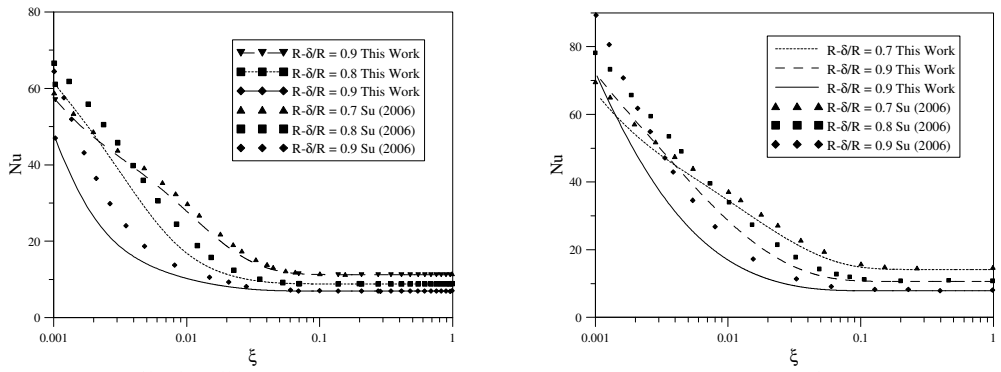

Prescribed wall temperature Bi =10

Figure 6: Comparison of Nusselt number obtained in this work and presented by Su (2006) using an analytical solution

The differences in the entry region can be attributed to some scaling problem in the ordinate axis originated in the definition of Pe. Although Su (2006) presents the definition of Pe in a clear way, this hypothesis has its origin in the fact that the curves are systematically shifted. If this problem didn't exist the curves would coincide exactly. Furthermore, the Nusselt numbers for the developed region are almost coincident as well, as shown Table 4.

Table 4: Nussel number at the developed region

	Nu_∞					
	TP		$Bi=2$		$Bi=10$	
$\frac{R-\delta}{R}$	This work	SU	This work	SU	This work	SU
0.7	11.27	11.26	18.57	19.02	14.16	14.47
0.8	8.85	8.84	13.99	14.08	10.64	10.69
0.9	6.86	6.95	9.74	9.74	7.87	7.87

7. FINAL REMARKS

A solution algorithm for the calculation of hydrodynamic and heat transfer parameters for two-phase annular flow was successfully implemented. It solves the triangular relationship between the film mass flow, wall shear stress and film thickness through an iterative procedure, taking advantage of the coupled solution of the core and the film velocity profiles. In this way, no empirical closure correlation is used, and no velocity profile is assumed beforehand for the film.

The hydrodynamic model was successfully validated for liquid-liquid systems with the analytical solution. In turn, the validation for the heat transfer problem shows the universality of the coupled solution of both phases using an equivalent diffusivity at the interface that accounts for the continuity of heat and momentum fluxes. Some deviations in the temperature profiles are observed in the cases where the physical properties were not known, which could have led to the slight differences in the results.

The solution algorithm presented in this work can be readily extended to deal with other annular flow patterns such as gas-liquid, evaporating film or any kind of turbulent flow, as long as the physical phenomena as entrainment and deposition, turbulence, etc. are properly incorporated into the algorithm.

8. REFERENCES

Adechy, D. & Issa, R.I., 2004. Modelling of annular flow through pipes and T-junctions. Comp. & Fluids, 33, 289-313.

Alipchenkov, V.M. et al., 2004. A three-fluid model of two-phase dispersed-annular flow. International Journal of Heat and Mass Transfer, 47(24), 5323-5338.

Antal, S.P. et al., 1998. The Development of Multidimensional Modeling Capabilities for Annular Flows. In Lyon, France.

Azzopardi, B.J., 1997. Drops in annular two-phase flow. Int. J. Multiphase Flow, 23, 1-53.

Bannwart, A.C., 2001. Modeling aspects of oil–water core–annular flows. J. of Petroleum Sc. & Eng., 32, 127 - 143.

Dobran, F., 1983. Hydrodynamic and Heat Transfer Analysis of Two-Phase Annular Flow With a New Liquid Film Model of Turbulence. International Journal of Heat and Mass Transfer, 26, 1159-1171.

Fernández, F, Alvarez Toledo, A., Paladino, E. E., 2010, Submitted to 13th Brazilian Congress of Thermal Sciences and Engineering - ENCIT 2010.

Fu, F. & Klausner, J.F., 1997. A separated flow model for predicting two-phase pressure drop and evaporative heat transfer for vertical annular flow. International Journal of Heat and Fluid Flow, 18(97), 541-549.

Ghosh, S. et al., 2009. Review of oil water core annular flow. Renewable and Sustainable Energy Reviews, 13, 1957-1965.

Hewitt, G.F. & Whalley, P.B., 1989. Vertical annular two-phase flow. Multiphase Sc. and Technology, 4, 103-181.

Kishore, B.N. & Jayanti, S., 2004. A multidimensional model for annular gas-liquid flow. Chem. Eng. Sci., 59, 3577-3589.

Leib, T.M., Fink, M. & Hasson, D., 1971. Heat transfer in vertical annular laminar flow of two immiscible liquids. Int. J. Multiphase Flow, 33, 533-549.

Moeck, E.O. & Stachiewicz, J.W., 1972. A droplet interchange model for annular-dispersed two-phase flow. Int. J. Heat Mass Transfer, 15, 637-653.

Okawa, T. et al., 2000. Numerical Simulation of Annular-Dispersed Flows in Round Tubes and Annuli Using a Multi-Fluid Model. In Third UK-Japan Mini-Seminar. Imperial College, London, UK.

Patankar, S.V. & Spalding, D.B., 1972. A calculation procedure for heat, mass and momentum transfer in three-dimensional parabolic flows. International Journal of Heat and Mass Transfer, 15(10), 1787-1806.

Patankar, S.V., 1980. Numerical Heat Transfer and Fluid Flow, Taylor & Francis.

Stockman, G. & Epstein, N., 2001. Uniform flux heat transfer in concentric laminar flow of two immiscible liquids. Can J Chem Eng, 79, 990–995.

Su, J., 2006. Exact Solution of Thermal Entry Problem in Laminar Core-annular Flow of Two Immiscible Liquids. Chemical Engineering Research and Design, 84(11), 1051-1058.

Whalley, R.B. & Hewitt, G.F., 1978. The correlation of liquid entrain- ment fraction and entrainment rate in annular two-phase flow.

9. RESPONSIBILITY NOTICE

The authors are the only responsible for the printed material included in this paper.